

# Effect of Image Forces on Polyelectrolyte Adsorption at a Charged Surface

René Messina\*

*Institut für Theoretische Physik II,  
Heinrich-Heine-Universität Düsseldorf,*

*Universitätsstrasse 1, D-40225 Düsseldorf, Germany*

(Dated: October 11, 2021)

## Abstract

The adsorption of flexible and highly charged polyelectrolytes onto oppositely charged planar surfaces is investigated by means of Monte Carlo simulations. The effect of image forces stemming from the dielectric discontinuity at the substrate interface is considered. The influence, at fixed polyelectrolyte volume fraction, of chain length and surface-charge density is also considered. A detailed structural study, including monomer and fluid charge distributions, is provided. It is demonstrated that image forces can considerably reduce the degree of polyelectrolyte adsorption and concomitantly inhibit the charge inversion of the substrate by polyelectrolytes.

PACS numbers: 82.35.Gh, 82.35.Rs, 61.20.Qg, 61.20.Ja

---

\*Electronic address: messina@thphy.uni-duesseldorf.de

## I. INTRODUCTION

The adsorption of charged polymers [polyelectrolytes (PEs)] on charged surfaces is an important phenomenon in industrial and biological processes. Recent model and well controlled experiments [1, 2] were devoted to characterize PE adsorptions. The understanding of PE adsorption remains an outstanding problem because of the many different typical interactions involved there: strong electrostatic substrate-PE binding, monomer-monomer (PE-PE) repulsion, chain-entropy, excluded volume, etc. Another complication arises from the *dielectric discontinuity* between the solvent and the substrate generating surface-polarization charges, which occurs in experimental situations.

On the theoretical side, PE adsorption on planar charged surfaces has been intensively studied by several authors [3, 4, 5, 6, 7, 8, 9, 10, 11, 12, 13, 14, 15, 16, 17, 18, 19, 20, 21, 22, 23, 24] on the level of mean field theories. The case of PE adsorption on heterogeneously charged surfaces was recently theoretically addressed by de Vries et al. [21]. A remarkable common feature of some of these studies is the charge reversal (*overcharging*) of the substrate by the adsorbed PEs (see e. g. Refs. [12, 13, 15, 16, 19, 25]). The PE adsorption onto *similarly* charged substrates were recently investigated by Dobrynin and Rubinstein [19] and Cheng and Lai [23, 24]. In the latter situation, the PE adsorption is then driven either by *non-electrostatic short range* forces [19] or *attractive image forces* [23, 24] stemming from a high-dielectric surface. The problem of *repulsive* image forces stemming from a low-dielectric surface was studied by Borisov et al. [9] and Netz and Joanny [16] on the level of the Debye-Hückel approximation.

As far as computer simulations are concerned, there exist few Monte Carlo (MC) studies about PE adsorption on planar charged substrates [23, 26, 27, 28, 29, 30]. The first MC study on PE adsorption was that of Beltán et al. [26] where a lattice-model was employed. Yamakov et al. [28] performed extensive MC simulations and found excellent agreement with the scaling predictions of Borisov et al. [9], where different regimes of adsorption are identified. Ellis et al. [29] considered the interesting case of heterogeneously charged surfaces (made of positively and negatively charged surface-sites) and demonstrated that a PE carrying the same sign of charge as that of the net charge of the substrate can adsorb. Cheng et al. [23] also investigated the effect of image charges on a high-dielectric constant substrate. It is to mention that all these MC simulations [23, 26, 27, 28, 29] use the Debye-

Hückel approximation. It is only for the case of PE multilayering studied by Messina [30] that unscreened long-range electrostatic interactions were properly treated.

In this article, we investigate multi-chain adsorption in the dilute regime but at fixed PE volume fraction in a salt-free environment. Counterions from the substrate and the PEs as well as image forces are explicitly taken into account. The influence of chain length (for short chains) and substrate-charge density is also considered. Our paper is organized as follows: The model and simulation technique are detailed in Sec. II. Our results are presented in Sec. III and Sec. IV provides concluding remarks.

## II. MODEL AND PARAMETERS

### A. Simulation model

The setup of the system under consideration is similar to that recently investigated with a planar substrate (without image forces) [30]. Within the framework of the primitive model we consider a PE solution near a charged hard wall with an implicit solvent (water at  $z > 0$ ) of relative dielectric permittivity  $\epsilon_s \approx 80$ . The substrate located at  $z < 0$  is characterized by a relative dielectric permittivity  $\epsilon_p$  which leads to a dielectric jump  $\Delta_\epsilon$  (when  $\epsilon_s \neq \epsilon_p$ ) at the interface defined as

$$\Delta_\epsilon = \frac{\epsilon_s - \epsilon_p}{\epsilon_s + \epsilon_p} \geq 0. \quad (1)$$

The *negative* bare surface-charge density of the substrate is  $-\sigma_0 e$ , where  $e$  is the (positive) elementary charge and  $\sigma_0 > 0$  is the number of charges per unit area. Electroneutrality is always ensured by the presence of explicit monovalent ( $Z_c = 1$ ) plate's counterions (i.e., monovalent cations) of diameter  $a$ . PE chains are made up of  $N_m$  *monovalent* positively charged monomers ( $Z_m = 1$ ) of diameter  $a$ . Their counterions (monovalent anions) are also explicitly taken into account with the same parameters up to to the charge sign as the monomers. Hence, all microions are monovalent:  $Z = Z_c = Z_m = 1$  with the same diameter size  $a$ .

All these particles making up the system are immersed in a rectangular  $L \times L \times \tau$  box. Periodic boundary conditions are applied in the  $(x, y)$  directions, whereas hard walls are present at  $z = 0$  (location of the charged interface) and  $z = \tau$  (location of an *uncharged* wall).

The total energy of interaction of the system can be written as

$$U_{tot} = \sum_i \left[ U_{hs}^{(plate)}(z_i) + U_{coul}^{(plate)}(z_i) \right] + \sum_{i,i < j} [U_{hs}(r_{ij}) + U_{coul}(\mathbf{r}_i, \mathbf{r}_j) + U_{FENE}(r_{ij}) + U_{LJ}(r_{ij})], \quad (2)$$

where the first (single) sum stems from the interaction between an ion  $i$  (located at  $z = z_i$ ) and the charged plate, and the second (double) sum stems from the pair interaction between ions  $i$  and  $j$  with  $r_{ij} = |\mathbf{r}_i - \mathbf{r}_j|$ . All these contributions to  $U_{tot}$  in Eq. (2) are described in detail below.

Excluded volume interactions are modeled via a hardcore potential [31] defined as follows

$$U_{hs}(r_{ij}) = \begin{cases} 0, & \text{for } r_{ij} \geq a \\ \infty, & \text{for } r_{ij} < a \end{cases} \quad (3)$$

for the microion-microion one, and

$$U_{hs}^{(plate)}(z_i) = \begin{cases} 0, & \text{for } a/2 \leq z_i \leq \tau - a/2 \\ \infty, & \text{otherwise} \end{cases} \quad (4)$$

for the plate-microion one. For clarity, we recall that a microion stands either for a (charged) monomer or a counterion.

The electrostatic energy of interaction between two microions  $i$  and  $j$  reads

$$\beta U_{coul}(\mathbf{r}_i, \mathbf{r}_j) = \pm l_B \left[ \frac{1}{r_{ij}} + \frac{\Delta_\epsilon}{\sqrt{x_{ij}^2 + y_{ij}^2 + (z_i + z_j)^2}} \right], \quad (5)$$

where  $+$ ( $-$ ) applies to microions of the same (opposite) sign,  $l_B = \beta e^2 / 4\pi\epsilon_0\epsilon_r$  is the Bjerrum length corresponding to the distance at which two protonic charges interact with  $1/\beta = k_B T$ , and  $\Delta_\epsilon$  is given by Eq. (1). The first term in Eq. (5) corresponds to the direct Coulomb interaction between real ions, whereas the second term represents the interaction between the real ion  $i$  and the image of ion  $j$ . By symmetry, the latter also describes the interaction between the real ion  $j$  and the image of ion  $i$  yielding an implicit factor 1/2. The electrostatic energy of interaction between an ion  $i$  and the (uniformly) charged plate reads

$$\beta U_{coul}^{(plate)}(z_i) = l_B \left[ \pm 2\pi\sigma_0 z_i + \frac{\Delta_\epsilon}{4z_i} \right], \quad (6)$$

where, for the first term,  $+$ ( $-$ ) applies to positively (negatively) charged ions. The second term in Eq.(6) stands for the *self-image* interaction, i.e., the interaction between the ion  $i$  and its own image. An appropriate and efficient modified Lekner sum was utilized to compute the electrostatic interactions with periodicity in *two* directions [32]. To link our simulation parameters to experimental units and room temperature ( $T = 298\text{K}$ ) we choose  $a = 4.25$  Å leading to the Bjerrum length of water  $l_B = 1.68a = 7.14$  Å. In order to investigate the effect of image forces we take a value of  $\epsilon_p = 2$  for the dielectric constant of the charged substrate (which is a typical value for silica or mica substrates [33]) and  $\epsilon_s = 80$  for that of the aqueous solvent yielding  $\Delta_\epsilon = \frac{80-2}{80+2} \approx 0.951$ . The case of identical dielectric constants  $\epsilon_p = \epsilon_s$  ( $\Delta_\epsilon = 0$ ) corresponds to the situation where there are no image charges.

The PE chain connectivity is modeled by employing a standard finite extendible nonlinear elastic (FENE) potential for good solvent, which reads

$$U_{FENE}(r) = \begin{cases} -\frac{1}{2}\kappa R_0^2 \ln \left[ 1 - \frac{r^2}{R_0^2} \right], & \text{for } r < R_0 \\ \infty, & \text{for } r \geq R_0 \end{cases} \quad (7)$$

with  $\kappa = 27k_B T/a^2$  and  $R_0 = 1.5a$ . The excluded volume interaction between chain monomers is taken into account via a shifted and truncated Lennard-Jones (LJ) potential given by

$$U_{LJ}(r) = \begin{cases} 4\epsilon \left[ \left( \frac{a}{r} \right)^{12} - \left( \frac{a}{r} \right)^6 \right] + \epsilon, & \text{for } r \leq 2^{1/6}a \\ 0, & \text{for } r > 2^{1/6}a \end{cases} \quad (8)$$

where  $\epsilon = k_B T$ . These parameter values lead to an equilibrium bond length  $l = 0.98a$ .

All the simulation parameters are gathered in Table I. The set of simulated systems can be found in Table II. The equilibrium properties of our model system were obtained by using standard canonical MC simulations following the Metropolis scheme [34, 35]. Single-particle moves were considered with an acceptance ratio of 30% for the monomers and 50% for the counterions. Depending on the parameters, the length of a simulation run ranges from  $2 \times 10^6$  up to  $7 \times 10^6$  MC steps per particle. Typically, about  $3 \times 10^5$  to  $2.5 \times 10^6$  MC steps were required for equilibration, and  $1 - 4 \times 10^6$  subsequent MC steps were used to perform measurements.

## B. Measured quantities

We briefly describe the different observables that are going to be measured. In order to study the PE adsorption, we compute the monomer density  $n(z)$  that is normalized as follows

$$\int_{a/2}^{\tau-a/2} n(z) L^2 dz = N_{PE} N_m. \quad (9)$$

To further characterize the PE adsorption, we also compute the total number of accumulated monomers  $\bar{N}(z)$  within a distance  $z$  from the planar charged plate that is given by

$$\bar{N}(z) = \int_{a/2}^z n(z') L^2 dz'. \quad (10)$$

It is useful to introduce the fraction of adsorbed monomers,  $N^*(z)$ , which is defined as follows

$$N^*(z) = \frac{\bar{N}(z)}{N_{PE} N_m}. \quad (11)$$

Another relevant quantity is the global *net fluid charge*  $\sigma(z)$  which is defined as follows

$$\sigma(z) = \int_{a/2}^z [n_+(z') - n_-(z')] dz', \quad (12)$$

TABLE I: List of key parameters with some fixed values.

Parameters	
$T = 298K$	room temperature
$\sigma_0 L^2$	charge number of the substrate
$\Delta_\epsilon = 0$ or $0.951$	dielectric discontinuity
$Z = 1$	microion valence
$a = 4.25 \text{ \AA}$	microion diameter
$l_B = 1.68a = 7.14 \text{ \AA}$	Bjerrum length
$L = 25a$	$(x, y)$ -box length
$\tau = 75a$	$z$ -box length
$N_{PE}$	number of PEs
$N_m$	number of monomers per chain

TABLE II: Simulated systems' parameters. The number of counterions (cations and anions) ensuring the overall electroneutrality of the system is not indicated.

System	$N_{PE}$	$N_m$	$\sigma_0 L^2$
$A$	96	2	64
$B$	48	4	64
$C$	24	8	64
$D$	12	16	64
$E$	6	32	64
$F$	12	16	32
$G$	12	16	128
$H$	12	16	192

where  $n_+$  and  $n_-$  stand for the density of all the positive microions (i.e., monomers and plate's counterions) and negative microions (i.e., PEs' counterions), respectively. It is useful to introduce the reduced surface charge density  $\sigma^*(z)$  defined as follows:

$$\sigma^*(z) = \frac{\sigma(z)}{\sigma_0}. \quad (13)$$

Thereby,  $\sigma^*(z)$  corresponds, up to a prefactor  $\sigma_0 e$ , to the net fluid charge per unit area (omitting the surface charge density  $-\sigma_0 e$  of the substrate) within a distance  $z$  from the charged wall. At the uncharged wall, electroneutrality imposes  $\sigma^*(z = \tau - a/2) = 1$ . By simple application of the Gauss' law,  $[\sigma^*(z) - 1]$  is directly proportional to the mean electric field at  $z$ . Therefore  $\sigma^*(z)$  can measure the *screening* strength of the substrate by the neighboring solute charged species.

### III. RESULTS AND DISCUSSION

From previous studies [9, 16, 36, 37] it is well understood that effects of image charges become especially relevant at sufficiently low surface charge density of the interface. It is also clear that the self-image interaction (*repulsive* for  $\Delta_\epsilon > 0$ , as is presently the case) is higher the higher the charge of the ions (polyions) since it scales like  $Z^2$ . In the present situation where we have to deal with PEs, the length of the chain ( $N_m$ ) is a key parameter

that can be seen as the valence of a polyion. Hence, we are going to study (i) the influence of chain length (Sec. III A) and (ii) that of surface charge density (Sec. III B). For the sake of consistency, we fixed the total number of monomers to  $N_{PE}N_m = 192$  meaning that the monomer concentration is *fixed* (see also Table II): The PE volume fraction  $\phi = \frac{4\pi}{3} \frac{N_{PE}N_m(a/2)^3}{L^2\tau} \approx 2.14 \times 10^{-3}$  is fixed.

### A. Influence of chain length

In this part, we consider the influence of chain length  $N_m$  at fixed surface charge density parameter  $\sigma_0 L^2 = 64$ . The latter corresponds experimentally to a moderate [2] surface charge density with  $-\sigma_0 e \approx -0.091$  C/m<sup>2</sup>. The chain length is varied from  $N_m = 2$  up to  $N_m = 32$  (systems *A* – *E*, see Table II). We have ensured that, for the longest chain with  $N_m = 32$ , size effects are still negligible since the end-to-end distance is about  $8.8a$  which is significantly smaller than  $L = 25a$  or  $\tau = 75a$ .

The profiles of the monomer distribution  $n(z)$  can be found in Fig. 1 and the corresponding microstructures are sketched in Fig. 2. Let us first comment the more simple case where no image charges are present [ $\Delta_\epsilon = 0$  - Fig. 1(a)]. For (very) short chains (here  $N_m \leq 4$ ), Fig. 1(a) shows that the density profiles exhibit a monotonic behavior *even near contact*. Within this regime of chain length, the monomer density near the charged wall increases with increasing  $N_m$ . This feature is fully consistent with the idea that stronger *lateral* correlations, the latter scaling like  $Z^{3/2}$  for spherical counterions at fixed  $\sigma_0$  [38, 39], induce a higher polyion adsorption. In other words, at (very) low  $N_m$  *conformational entropic* effects are not dominant and the short-chains systems can be qualitatively understood with the picture provided by spherical (or point-like) ions. The scenario becomes qualitatively different at higher chain length [here  $N_m \geq 8$  - see Fig. 1(a)], where  $n(z)$  presents a maximum near contact which is the signature of a *short range repulsion* that was also theoretically predicted by Borukhov et al. [10]. This non-trivial feature can be explained in terms of entropy: Near the surface of the substrate the number of available PE conformations is considerably reduced yielding to an entropic repulsion that can be detected if the driving force of PE adsorption (crucially controlled by  $\sigma_0$ ) is not strong enough. This latter statement will be properly examined and confirmed in Sec. III B where the influence of  $\sigma_0$  is addressed. Nonetheless, the highest value of  $n(z; N_m)$  increases with  $N_m$  as it should be. All

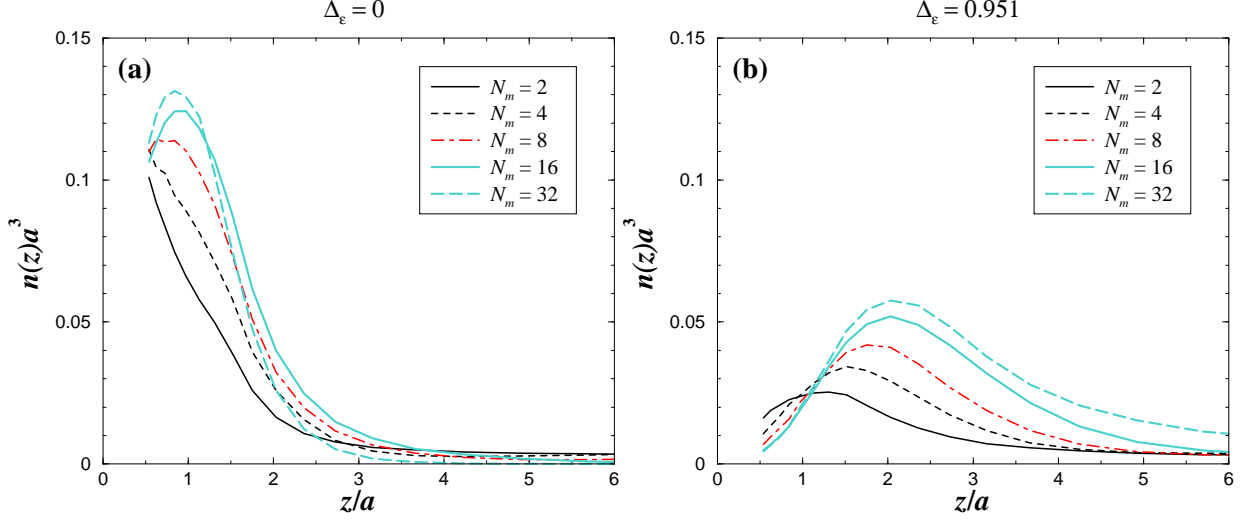


FIG. 1: Profiles of the monomer density  $n(z)$  for different chain length  $N_m$  with  $\sigma_0 L^2 = 64$  (systems  $A - E$ ). (a)  $\Delta_\epsilon = 0$ . (b)  $\Delta_\epsilon = 0.951$ .

these mentioned features can be visualized on the microstructures depicted in Fig. 2. One can summarize those relevant findings, valid for small enough  $\sigma_0$  and  $\Delta_\epsilon = 0$ , as follows:

- For very short chains the PE adsorption is similar to that occurring with spherical electrolytes.
- PE chains experience a short range repulsion near the substrate due to conformational entropic effects.

We now turn to the more complicated situation where image forces are present [ $\Delta_\epsilon = 0.951$  - Fig. 1(b)]. An immediate remark that can be drawn from a comparison with the  $\Delta_\epsilon = 0$  case is that the PE adsorption is much weaker due to the repulsive image-polyion interactions. At all  $N_m$ ,  $n(z)$  presents a maximum at  $z = z^*$  that is gradually shifted to larger  $z$  with increasing  $N_m$ . In other words, the *thickness* of the adsorbed PE layer as determined by  $z^*$  increases with  $N_m$ . This phenomenon is of course due to the fact that the image-polyion repulsion increases with  $N_m$ , similarly to what happens with multivalent (point-like or spherical) counterions [36, 37]. On the other hand, interestingly, the monomer density at contact *decreases* with increasing  $N_m$ . This is the result of a *combined* effect of (i) conformational entropy as explained above and (ii) the  $N_m$ -induced image-polyion repulsion. All those features are well illustrated on the microstructures of Fig. 2.

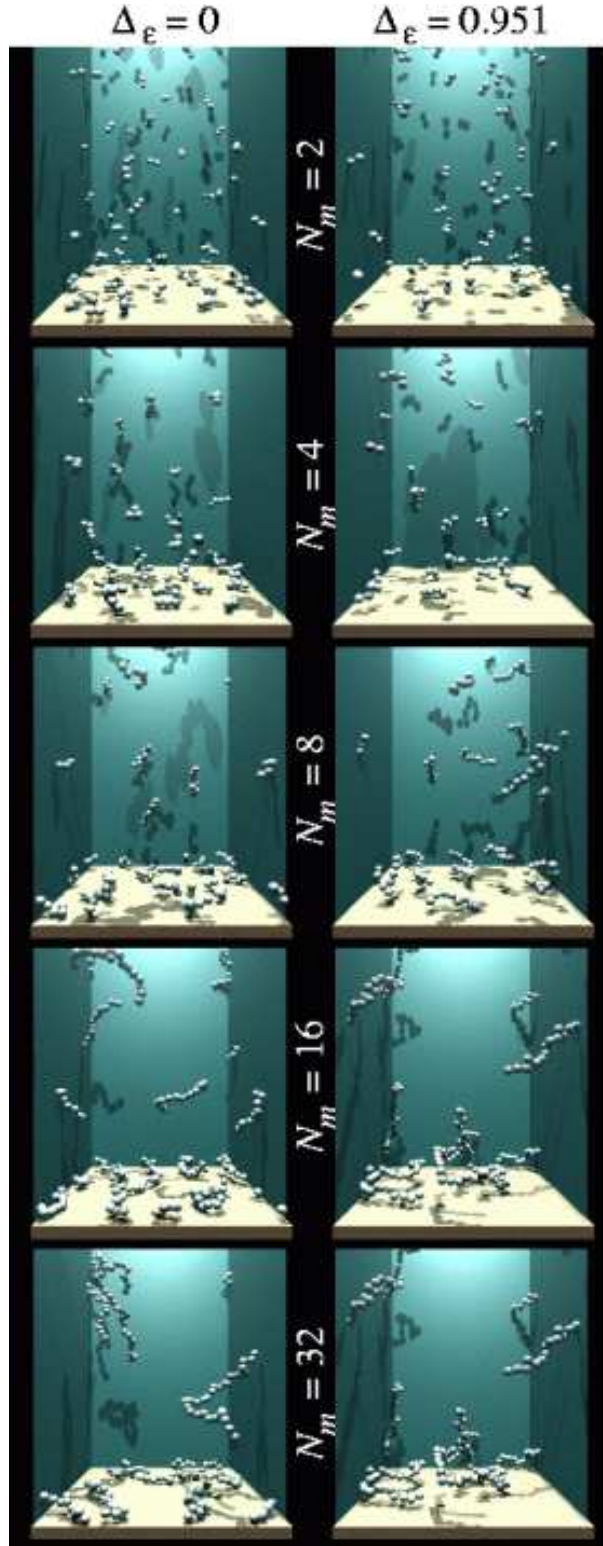


FIG. 2: Typical equilibrium microstructures of systems  $A - E$ . The little counterions are omitted for clarity.

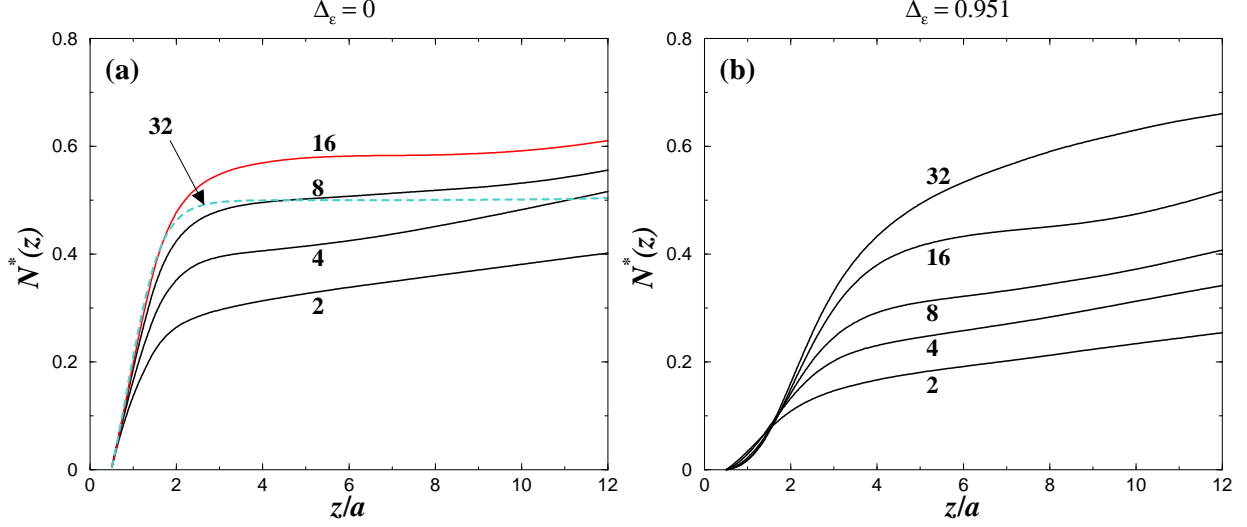


FIG. 3: Profiles of the fraction of adsorbed monomers  $N^*(z)$  for different chain length  $N_m$  (as indicated by its numerical value) with  $\sigma_0 L^2 = 64$  (systems A – E). (a)  $\Delta_\epsilon = 0$ . (b)  $\Delta_\epsilon = 0.951$ .

To gain further insight into the properties of PE adsorption, we have plotted the fraction of adsorbed monomers  $N^*(z)$  [Eq. (11)] in Fig. 3. At  $\Delta_\epsilon = 0$  [Fig. 3(a)], it is observed in the immediate vicinity of the wall (roughly for  $z \lesssim 1.5a$ ) that  $N^*(z; N_m)$  increases monotonically with  $N_m$  as expected. However, further away from the wall, a non-trivial effect is found where  $N^*(z; N_m)$  surprisingly exhibits a non-monotonic behavior with respect to  $N_m$ . More explicitly, in the regime of large  $N_m$  we have  $N^*(z; N_m = 32)$  that is clearly smaller than  $N^*(z; N_m = 16)$  and even smaller than  $N^*(z; N_m = 8)$  when one is sufficiently far from the wall. This remarkable phenomenon is going to be explained later by advocating the role of overcharging. Upon switching the image forces on [ $\Delta_\epsilon = 0.951$  - Fig. 3(b)],  $N^*(z; N_m)$  shows a qualitatively different behavior than that found at  $\Delta_\epsilon = 0$ , in accordance with our study concerning  $n(z)$ . More precisely: (i) very close to the wall,  $N^*(z; N_m)$  *decreases* with  $N_m$  whilst (ii) sufficiently far away from the wall  $N^*(z; N_m)$  *increases* with  $N_m$ . This behavior is fully consistent with our mechanisms previously discussed for  $n(z)$ . Below, we are going to show that the reduced net fluid charge  $\sigma^*(z)$  is a key observable to account for those reported properties of  $N^*(z; N_m)$ .

A deeper understanding of the physical mechanisms involved in PE adsorption can be gained by considering the net fluid charge parameter  $\sigma^*(z)$  [Eq. (13)] that describes the screening of the charged interface. The profiles of  $\sigma^*(z)$  for different  $N_m$  can be found in

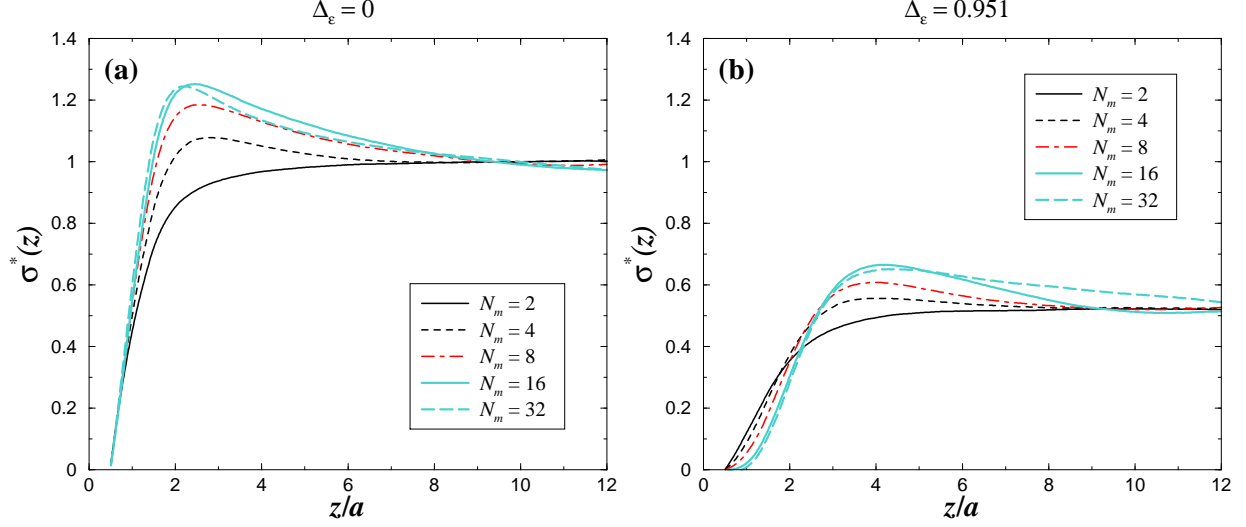


FIG. 4: Profiles of the reduced net fluid charge  $\sigma^*(z)$  for different chain length  $N_m$  with  $\sigma_0 L^2 = 64$  (systems A – E). (a)  $\Delta_\epsilon = 0$ . (b)  $\Delta_\epsilon = 0.951$ .

Fig. 4. At  $\Delta_\epsilon = 0$  [see Fig. 4(a)], it is shown that for long enough chains (here  $N_m \geq 4$ ) the substrate gets locally *overcharged* as signaled by  $\sigma^*(z) > 1$ . Physically, this means that the global local charge of the adsorbed monomers [40] is larger in absolute value than that of the plate's charge. In other words, the plate is *overscreened* by the adsorbed PE chains. Fig. 4(a) indicates that the degree of overcharging increases with  $N_m$  as expected from the behavior of multivalent counterions, and seems to saturate at high  $N_m$ . This enhanced  $N_m$ -overcharging leads to a sufficiently strong effective repulsion between the substrate and the PEs in the solution, which in turn prevents from further adsorption. It is precisely this mechanism that explains the apparent anomaly found in Fig. 3(a) where, sufficiently away from the surface, it was reported a significantly lower monomer fraction  $N^*(z; N_m)$  at  $N_m = 32$  than at  $N_m = 16$  or  $N_m = 8$ . This spectacular effect is well illustrated in Fig. 2 (with  $N_m = 32$ ) where, above the (strongly bound) adsorbed PEs, there is a depletion region leading to a plateau in  $N^*(z; N_m = 32)$ .

Upon inducing polarization charges [ $\Delta_\epsilon = 0.951$  - Fig. 4(b)] overscreening is canceled. This, in turn, accounts for the absence of plateau in  $N^*(z; N_m)$  at  $\Delta_\epsilon = 0.951$ . That striking disappearance of overcharging can be rationalized by establishing again an analogy with multivalent spherical ions:

- For the sake of simplicity, let us assume that the PE can be electrostatically envisioned

as a spherical polyion of valence  $N_m$  with a radius corresponding roughly to the radius of gyration of the chain. Thereby, the image-polyion *repulsive* interactions [including the self-image repulsion as well as the lateral image-ion correlations as given by the second term of Eq. (5)] scale like  $N_m^2$  whereas the *attractive* driving force of polyion adsorption due to Wigner crystal ordering scales like  $N_m^{3/2}$  [37]. The latter driving force corresponds to the highest possible attraction between the substrate and the polyion and is therefore a good candidate for the present discussion. Consequently, at large enough  $N_m$  image forces will be dominant and inhibit overcharging.

## B. Influence of substrate surface-charge density

To complete our investigation, we would like to address the influence of the substrate charge density on the PE adsorption in presence of image forces. In this respect, we consider (at fixed  $N_m = 16$ ) three additional values of the charge density:  $\sigma_0 L^2 = 32, 128, 192$  corresponding to the systems  $F, G, H$ , respectively (see Table II).

The plots of the monomer density  $n(z)$  at various values of  $\sigma_0 L^2$  can be found in Fig. 5. Microstructures of systems  $F$  and  $H$  are presented in Fig. 6. At  $\Delta_\epsilon = 0$  [see Fig.

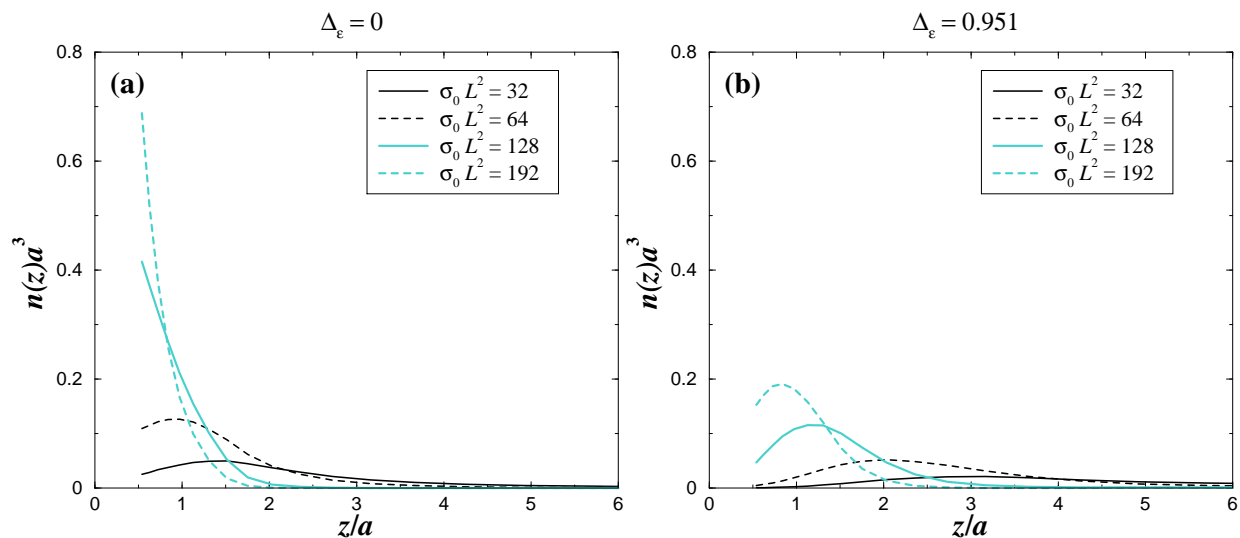


FIG. 5: Profiles of the monomer density  $n(z)$  for different parameters of surface charge density  $\sigma_0 L^2$  with  $N_m = 16$  (systems  $D, F - H$ ). The case  $\sigma_0 L^2 = 64$  (system  $D$ ) from Fig. 1 is reported here again for easier comparison. (a)  $\Delta_\epsilon = 0$ . (b)  $\Delta_\epsilon = 0.951$ .

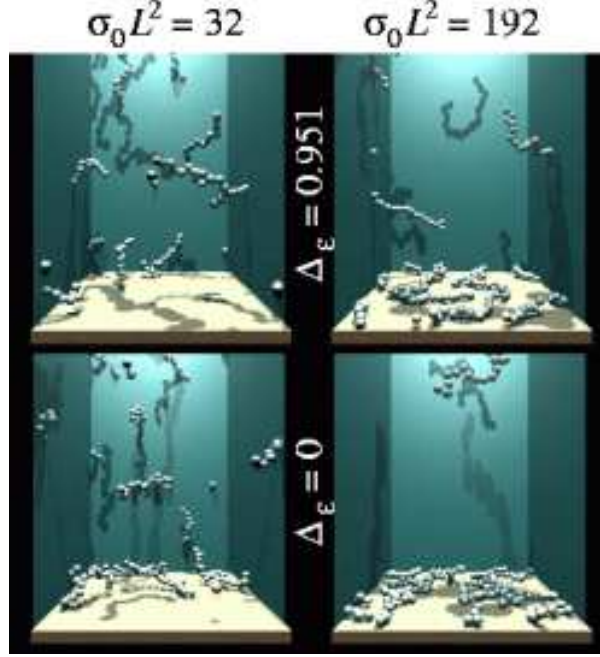


FIG. 6: Typical equilibrium microstructures of systems  $F$  and  $H$ . The little counterions are omitted for clarity.

5(a)], the monomer density at contact increases with  $\sigma_0$  as it should be. Interestingly, the local maximum in  $n(z)$  [present at small  $\sigma_0$  (here  $\sigma_0 L^2 \leq 64$ )] *vanishes at large  $\sigma_0$*  [see Fig. 5(a)]. This feature is the result of a  $\sigma_0$ -enhanced driving force of adsorption that overcomes entropic effects at large enough  $\sigma_0$ . The strong adsorption at  $\sigma_0 L^2 = 192$  leads to a *flat* PE layer as well illustrated in Fig. 6.

By polarizing the substrate surface ( $\Delta_\epsilon = 0.951$ ), it can be seen from Fig. 5(b) and the snapshot of Fig. 6 that there is a strong monomer depletion near contact at  $\sigma_0 L^2 = 32$ . This feature is due to the combined effects of (i) conformational entropy, (ii) image-monomer repulsion and (iii) a lower electrostatic wall-monomer attraction. Upon increasing  $\sigma_0$  the monomer density near contact becomes larger, and concomitantly, the maximum in  $n(z)$  is systematically shifted to smaller  $z$ . It is to say that the thickness of the adsorbed PE layer decreases with  $\sigma_0$ .

The profiles of  $N^*(z)$  are provided in Fig. 7 from which further characterization of PE adsorption can be obtained. At  $\Delta_\epsilon = 0$ , Fig. 7(a) indicates that  $N^*(z; \sigma_0)$  increases with  $\sigma_0$  but saturates at high  $\sigma_0$ . This latter saturation effect should only be relevant for a regime of charge where  $\eta \equiv \frac{N_{PE} N_m}{\sigma_0 L^2}$  is about unity. Indeed, in a typical experimental situation at finite

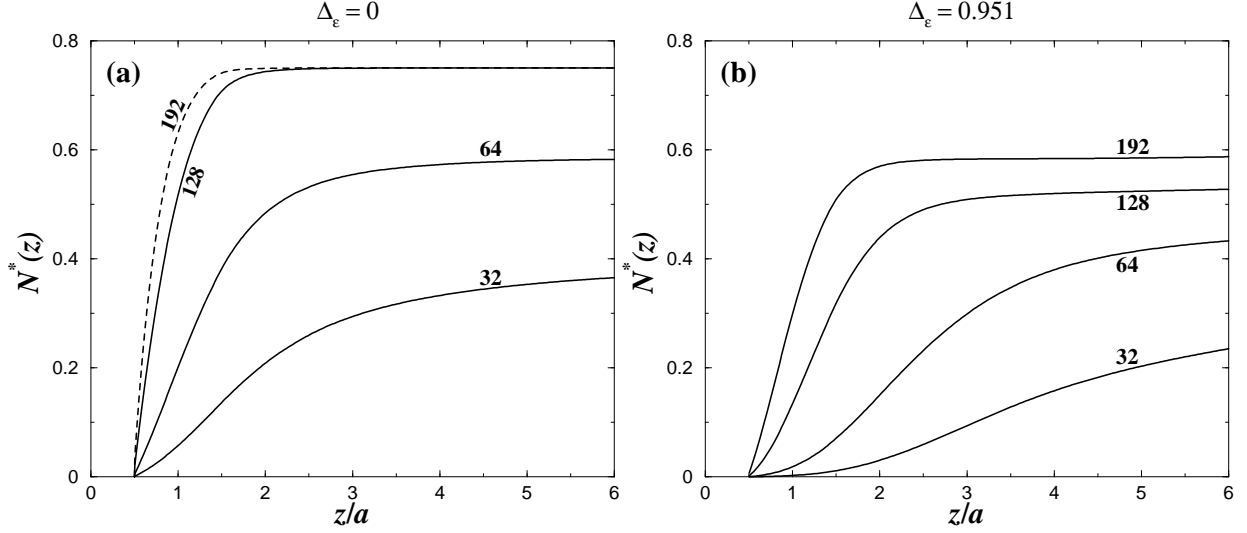


FIG. 7: Profiles of the fraction of adsorbed monomers  $N^*(z)$  for different parameters of surface charge density  $\sigma_0 L^2$  (as indicated by its numerical value) with  $N_m = 16$  (systems  $D, F - H$ ). The case  $\sigma_0 L^2 = 64$  (system  $D$ ) from Fig. 3 is reported here again for easier comparison. (a)  $\Delta_\epsilon = 0$ . (b)  $\Delta_\epsilon = 0.951$ .

monomer concentration (even in the dilute regime) we have  $\eta \gg 1$  so that overcharging is always possible at large  $\sigma_0$  and thereby  $N^*(z; \sigma_0)$  should always significantly increase with  $\sigma_0$  as long as packing effects (as generated by the excluded volume of the monomers) are not vivid. In parallel, the plateau reported at  $\sigma_0 L^2 = 128$  and  $\sigma_0 L^2 = 192$  in Fig. 7(a), is the signature of a monomer depletion above the adsorbed PE layer (see also Fig. 6) due to a strong screening of the surface charge by the latter. At  $\Delta_\epsilon = 0.951$ , Fig. 7(b) shows that  $N^*(z)$  is considerably smaller than at  $\Delta_\epsilon = 0$  even for high  $\sigma_0$ , in accordance with the behavior of  $n(z)$  from Fig. 5. The  $\Delta_\epsilon$ -induced desorption is especially strong at  $\sigma_0 L^2 = 32$  where the image-monomer repulsion clearly counterbalances the electrostatic wall-monomer attraction. More quantitatively, at  $z = 3a$  (a  $z$ -distance corresponding roughly to the radius of gyration of the chain with  $N_m = 16$ ) about 30% [i.e.,  $N^*(z) = 0.3$ ] of the monomers are adsorbed with  $\Delta_\epsilon = 0$  against only 10% with  $\Delta_\epsilon = 0.951$  [see Fig. 7(b)].

#### IV. CONCLUDING REMARKS

We first would like to make some final remarks about the presented results. As far as the charge surface distribution on the substrate's surface is concerned, we have assumed a *smeared-out* one in contrast to real experimental situation where it is *discrete*. Previous numerical studies [41, 42, 43] have shown that the counterion distribution at inhomogeneously charged substrates may deviate from that obtained at smeared-out ones at strong Coulomb coupling (i.e., multivalent counterions and/or high Bjerrum length) or strong substrate charge modulations. Nonetheless, at standard Bjerrum length (i.e.,  $l_B = 7.1$  Å for water at room temperature as is presently the case) and with discrete monovalent ions generating the substrate's surface charge, it has been demonstrated that the counterion distribution is marginally modified [41] even for trivalent counterions. Hence, we think that our results will not qualitatively differ from the more realistic situation of non-smeared-out substrate charges consisting of discrete monovalent ions.

An other approximation in our model is the location of the dielectric discontinuity. More precisely, it was implicitly assumed that the latter coincides with the charged interface (considered here as a hard wall). In fact, experimentally, it is not clear where the dielectric discontinuity is located and the transition is rather gradual and spreads out over several Angströms [44], so that in a continuum description the dielectric discontinuity might be located somewhat below the *hard* interface. In this respect our model tends to slightly overestimate the effect of image forces and namely, with  $\Delta_\epsilon > 0$ , the self-image *repulsion*. Furthermore, in the presence of *short-range* attractive interactions between the substrate and the PEs (for instance stemming from some specific chemical properties of the chains and the substrate, i.e. chemisorption), the effect of image charges might also be reduced [19]. This means that the substrate-charge *undercompensation* by PEs induced by repulsive image forces as reported in Fig. 4(b) is dependent on the relative strength of that short-range attractive interaction, which is not taken into account in our model. Nevertheless, we are confident that our results provide a reliable fingerprint for the understanding of the effect of image forces on PE adsorption in a salt-free environment.

It is not a straightforward task to access experimentally to these effects stemming from image forces. One major difficulty arises from the fact that by changing the dielectric constant of the solvent,  $\epsilon_1$ , one changes the degree of ionization of the PEs. However, there

is the experimental possibility to tune  $\Delta_\epsilon$  by using *organic* solvents (i.e., with a low  $\epsilon_1$  but still polar) with a mixture of large colloidal particles [e.g., latex particles with weak curvature and (low) dielectric constant  $\epsilon_2$  such that  $\epsilon_2 \leq \epsilon_1$ ] and PEs. In this experimental context, one should be able to verify the trends of our current findings.

To conclude, we have performed MC simulations to address the effect of image forces on PE adsorption at oppositely charged planar substrates. The influence of chain length and surface-charge density was also considered. We have considered a finite monomer concentration in the dilute regime for relatively short chains. Our main findings can be summarized as follows:

- For very short chains (here  $N_m \leq 4$ ) and with no image forces (i.e.,  $\Delta_\epsilon = 0$ ), the PE adsorption is similar to that occurring with little (spherical) multivalent counterions. For longer chains (here  $N_m \geq 8$ ), the PEs experience (even at  $\Delta_\epsilon = 0$ ) a short range repulsion near the substrate due to chain entropy effects. This latter feature is especially relevant at low substrate charge  $\sigma_0$ .
- At fixed  $\sigma_0$  and in the presence of repulsive *image forces* (here  $\Delta_\epsilon = 0.951$ ), it was demonstrated that the monomer depletion in the vicinity of the substrate as well as the thickness of the PE layer grow with chain length  $N_m$ . Concomitantly, the *charge reversal* of the substrate by the adsorbed PEs *vanishes*.
- Upon varying  $\sigma_0$  at fixed  $N_m$ , it was shown at  $\Delta_\epsilon = 0$  that the net substrate-PE force becomes purely attractive at sufficiently high  $\sigma_0$ , where chain-entropy effects are overcompensated. When image forces are present, the PE *depletion* near the substrate as well as the thickness of the adsorbed PE layer decrease with  $\sigma_0$ .

A future work will address the adsorption of stiff *rod*-like PEs. This very interesting situation was recently theoretically examined by Cheng and de la Cruz [22]. Numerical simulation data would be of great help to further characterize the transversal and in-plane structures as well as to elucidate the influence of image forces.

## Acknowledgments

The author thanks H. Löwen for enlightening discussions. The SFB TR6 is acknowledged for financial support.

---

- [1] N. Hansupalak and M. M. Santore, *Langmuir* **19**, 7423 (2003).
- [2] A. Tulpar and W. A. Ducker, *J. Phys. Chem. B* **108**, 1667 (2004).
- [3] F. W. Wiegel, *J. Phys. A: Math. Gen.* **10**, 299 (1977).
- [4] H. A. Van der Schee and J. Lyklema, *J. Phys. Chem.* **88**, 6621 (1984).
- [5] M. Muthukumar, *J. Chem. Phys.* **86**, 7230 (1987).
- [6] M. R. Böhmer, O. A. Evers, and J. M. H. M. Scheutjens, *Macromolecules* **23**, 2288 (1990).
- [7] R. Varoqui, A. Johnner, and A. Elaissari, *J. Chem. Phys.* **94**, 6873 (1991).
- [8] R. Varoqui, *J. Phys. II* **3**, 1097 (1993).
- [9] O. V. Borisov, E. B. Zhulina, and T. M. Birshtein, *J. Phys. II* **4**, 913 (1994).
- [10] I. Borukhov, D. Andelman, and H. Orland, *Europhys. Lett.* **32**, 499 (1995).
- [11] X. Châtelier and J.-F. Joanny, *J. Phys. II* **6**, 1669 (1996).
- [12] P. Linse, *Macromolecules* **29**, 326 (1996).
- [13] V. Shubin and P. Linse, *Macromolecules* **30**, 5944 (1997).
- [14] I. Borukhov, D. Andelman, and H. Orland, *Macromolecules* **31**, 1665 (1998).
- [15] J. F. Joanny, *Eur. Phys. J. B* **9**, 117 (1999).
- [16] R. R. Netz and J. F. Joanny, *Macromolecules* **32**, 9013 (1999).
- [17] A. V. Dobrynin, A. Deshkovski, and M. Rubinstein, *Phys. Rev. Lett.* **84**, 3101 (2000).
- [18] A. V. Dobrynin, A. Deshkovski, and M. Rubinstein, *Macromolecules* **34**, 3421 (2001).
- [19] A. V. Dobrynin and M. Rubinstein, *J. Phys. Chem. B* **107**, 8260 (2003).
- [20] A. Shafir, D. Andelman, and R. R. Netz, *J. Chem. Phys.* **119**, 2355 (2003).
- [21] R. de Vries, F. Weinbreck, and C. G. de Kruif, *J. Chem. Phys.* **118**, 4649 (2003).
- [22] H. Cheng and O. de la Cruz, *J. Chem. Phys.* **119**, 12635 (2003).
- [23] C.-H. Cheng and P.-Y. Lai, [arxiv:cond-mat/0312315](#).
- [24] C.-H. Cheng and P.-Y. Lai, [arxiv:cond-mat/0403722](#).
- [25] A. Y. Grosberg, T. T. Nguyen, and B. I. Shklovskii, *Rev. Mod. Phys.* **74**, 329 (2002).

- [26] S. Beltrán, H. H. Hooper, H. W. Blanch, and J. M. Prausnitz, *Macromolecules* **24**, 3178 (1991).
- [27] C. Y. Kong and M. Muthukumar, *J. Chem. Phys.* **109**, 1522 (1998).
- [28] V. Yamakov, A. Milchev, O. Borisov, and B. Dunweg, *J. Phys.-Condens. Mat.* **11**, 9907 (1999).
- [29] M. Ellis, C. Y. Kong, and M. Muthukumar, *J. Chem. Phys.* **112**, 8723 (2000).
- [30] R. Messina, *Macromolecules* **37**, 621 (2004).
- [31] Only the monomer-monomer excluded volume interaction was not modelled by a hard-sphere potential. There, a purely repulsive Lennard-Jones potential was used.
- [32] A. Grzybowski and A. Brodka, *Molec. Phys.* **100**, 1017 (2002).
- [33] M. D. Malinsky, K. L. Kelly, G. C. Schatz, and R. P. van Duyne, *J. Phys. Chem. B* **105**, 2343 (2001).
- [34] N. Metropolis *et al.*, *J. Chem. Phys.* **21**, 1087 (1953).
- [35] M. P. Allen and D. J. Tildesley, *Computer Simulations of Liquids* (Clarendon Press, Oxford, 1987).
- [36] G. M. Torrie, J. P. Valleau, and G. N. Patey, *J. Chem. Phys.* **76**, 4615 (1982).
- [37] R. Messina, *J. Chem. Phys.* **117**, 11062 (2002).
- [38] B. Shklovskii, *Phys. Rev. E* **60**, 5802 (1999).
- [39] R. Messina, C. Holm, and K. Kremer, *Phys. Rev. E* **64**, 021405 (2001).
- [40] Near the wall, the presence of the counterions at  $\Delta_\epsilon = 0$  is marginal so that the fluid charge is quasi exclusively provided by the charges of the adsorbed monomers. This becomes especially vivid when  $N_m \geq 4$  where overcharging occurs.
- [41] R. Messina, *Physica A* **308**, 59 (2002).
- [42] E. Allahyarov, H. Löwen, A. A. Louis, J.-P. Hansen, *Europhys. Letters* **57**, 731 (2002).
- [43] A. G. Moreira and R. R. Netz, *Europhys. Lett.* **57**, 911 (2002).
- [44] P. Linse, *J. Phys. Chem.* **90**, 6821 (1986).